ECCOMAS Congress 2016
VII European Congress on Computational Methods in Applied Sciences and Engineering
M. Papadrakakis, V. Papadopoulos, G. Stefanou, V. Plevris (eds.)
Crete Island, Greece, 5–10 June 2016

CONVERGENCE ANALYSIS OF COUPLING ITERATIONS FOR THE UNSTEADY TRANSMISSION PROBLEM WITH MIXED DISCRETIZATIONS

Azahar Monge[1] **and Philipp Birken**[1]

[1]Centre for Mathematical Sciences
Lund University
Box 118, 22100, Lund, Sweden
e-mail: azahar.monge@na.lu.se, web page: http://www.maths.lu.se/staff/azahar-monge

Keywords: Thermal Fluid Structure Interaction, Coupled Problems, Transmission Problem, Fixed Point Iteration, Dirichlet-Neumann Iteration

Abstract. *We analyze the convergence rate of the Dirichlet-Neumann iteration for the fully discretized one dimensional unsteady transmission problem. Specifically, we consider the coupling of two linear heat equations on two identical non overlapping intervals. The Laplacian is discretized using finite differences on one interval and finite elements on the other and the implicit Euler method is used for the time discretization. Following previous analysis where finite elements where used on both subdomains, we provide an exact formula for the spectral radius of the iteration matrix for this specific mixed discretizations. We then show that these tend to the ratio of heat conductivities in the semidiscrete spatial limit, but to a factor of the ratio of the products of density and specific heat capacity in the semidiscrete temporal one. In the previous finite element analysis, the same result was obtained in the semidiscrete spatial limit but the factor in the temporal limit was lower. This explains the fast convergence previously observed for cases with strong jumps in the material coefficients. Numerical results confirm the analysis.*

1 INTRODUCTION

Thermal fluid structure interaction occurs when a heat flux from a fluid leads to temperature changes in a structure or vice versa. Examples for this are cooling of gas-turbine blades, cooling of rocket thrust chambers [11, 12], thermal anti-icing systems of airplanes [4], supersonic reentry of vehicles from space [10, 14] or gas quenching [8, 19].
Unsteady thermal fluid structure interaction is modelled using two partial differential equations describing a fluid and a structure on different domains. The equations are coupled at an interface to model the heat transfer between fluid and structure. The standard algorithm to find solutions of the coupled problem is the Dirichlet-Neumann iteration, where the PDEs are solved separately using Dirichlet-, respectively Neumann boundary conditions with data given from the solution of the other problem. The convergence rate of the method has been analyzed in any standard book on domain decomposition method, e.g. [18, 20]. There, the iteration matrix is derived in terms of the spatial discretization matrices and the convergence rate is the spectral radius of that. However, this does not provide a quantitative answer, since the spectral radius is unknown.
We consider the transmission problem because it is a basic building block in fluid structure interaction. For this case, a one dimensional stability analysis was presented by Giles [7]. There, an explicit time integration method was chosen with respect to the interface unknowns. Henshaw and Chand provided in [9] a method to analyze stability and convergence speed of the Dirichlet-Neumann iteration in 2D based on applying the continuous Fourier transform to the semi-discretized equations. Their result depends on ratios of thermal conductivities and diffusivities of the materials. This is similar to the situation in [1, 5] where the performance of the coupling for incompressible fluids is affected by the added mass effect. However, in the fully discrete case we observe that the iteration converges much faster for some choices of materials [3], and that the speed of the iteration does not depend on the thermal diffusivities in some cases. In [16] the discrete case was analyzed for finite element discretizations. In this paper, we present a similar one dimensional analysis in the case of specific mixed discretizations.
Thus, we consider a complete discretization of the coupled problem using finite differences on one domain and finite elements on the other (in space) and the implicit Euler method in time. Then, we compute the spectral radius of the iteration matrix exactly in terms of the eigendecomposition of the resulting matrices for the one dimensional case. The asymptotics of the convergence rates when approaching the continuous case in either time or space are also computed resulting in the ratio of the thermal conductivities in space and a factor of the ratio of the heat capacities in time. These results are consistent with our numerical experiments.
An outline of the paper now follows. In Section 2, we define the problem to be solved in terms of the partial differential equations, boundary conditions and interface conditions. We also give a description of the discretization. In Section 3, we explain the Dirichlet-Neumann model. Our analysis for the discrete case of the model problem using Dirichlet-Neumann interface conditions for mixed discretizations is presented in Section 4. In Section 5, we present numerical results that show the theoretical stability analysis.

2 MODEL PROBLEM

The unsteady transmission problem is as follows, where we consider a domain $\Omega \subset \mathbb{R}^d$ which is cut into two subdomains $\Omega = \Omega_1 \cup \Omega_2$ with transmission conditions at the interface $\Gamma = \Omega_1 \cap \Omega_2$:

$$\begin{aligned}
\alpha_m \frac{\partial u_m(\mathbf{x},t)}{\partial t} + \lambda_m \Delta u_m(\mathbf{x},t) = f(x), \;\; t \in [t_0, t_f], \;\; \mathbf{x} \in \Omega_m \subset \mathbb{R}^d, \; m = 1,2, \\
u_m(\mathbf{x},y) = 0, \;\; t \in [t_0, t_f] \;\; \mathbf{x} \in \partial\Omega_m \backslash \Gamma, \\
u_1(\mathbf{x},y) = u_2(\mathbf{x},y), \;\; \mathbf{x} \in \Gamma, \\
\lambda_1 \partial_x u_1(\mathbf{x},y) \cdot \mathbf{n} = \lambda_2 \partial_x u_2(\mathbf{x},y) \cdot \mathbf{n}, \;\; \mathbf{x} \in \Gamma, \\
u_m(\mathbf{x},0) = u_m^0(\mathbf{x}), \;\; \mathbf{x} \in \Omega_m.
\end{aligned} \tag{1}$$

where $\mathbf{n}$ denotes the normal vector and we consider $d = 1, 2$.
The constants λ_1 and λ_2 describe the thermal conductivities of the materials on Ω_1 and Ω_2 respectively. $\alpha_m = \rho_m C_m$ where ρ_m respresents the density and C_m the heat capacity of the material placed in Ω_m, $m = 1, 2$. D_1 and D_2 represent the thermal diffusivities of the materials and they are defined by

$$D_m = \frac{\lambda_m}{\alpha_m}. \tag{2}$$

We consider a constant mesh width of $\Delta x = 1/(N+1)$ with N being the number of interior space discretization points in both Ω_1 and Ω_2. Moreover, we discretize this problem using a finite difference method (FDM) on Ω_1 and a finite element method (FEM) on Ω_2. The implicit Euler method is used for the time discretization.

2.1 Space Discretization

First of all, we focus on the FDM formulation on Ω_1 of problem (1). For this, let $\mathbf{u}_I^{(1)}$ correspond to the unknowns on Ω_1 and $\mathbf{u}_\Gamma$ correspond to the unknows at the interface Γ. From now on we assume that $f_1 = 0$ in order to simplify the analysis.
Then, applying second order central differences

$$\Delta u_1(x_i,t) \approx \frac{1}{\Delta x^2}(u_1(x_{i+1},t) - 2u_1(x_i,t) + u_1(x_{i-1},t)), \;\; \text{for } \; i = 1,..,N, \tag{3}$$

to approximate the second order spatial derivative of (1) for $m = 1$, we can write the resulting discrete system as:

$$\alpha_1 \dot{\mathbf{u}}_I^{(1)} + \mathbf{A}_1 \mathbf{u}_I^{(1)} + \mathbf{A}_{I\Gamma}^{(1)} \mathbf{u}_\Gamma = \mathbf{0}. \tag{4}$$

$\mathbf{A}_1$ corresponds to the discretization of the Laplacian operator on Ω_1 and the required data from the interface is inserted in the equation by the matrix $\mathbf{A}_{I\Gamma}^{(1)}$.
On the other hand, we also need to discretize the problem on Ω_2 using FEM formulation. For this, we choose an approximation U_2 of u_2 in a finite-dimensional subspace S^N of H^1 having the form

$$U_2(\mathbf{x},t) = \sum_{j=1}^{N-1} c_j(t)\phi_j(x). \tag{5}$$

where N is the number of interior spatial discretization points on Ω_2, c_j are the coefficient functions and ϕ_j the test functions. Then, the Galerkin finite element problem is to determine $U_2 \in S^N$ such that

$$\begin{aligned} \alpha_2 \int_{\Omega_2} \frac{\partial U_2}{\partial t}\phi_j dV + \lambda_2 \int_{\Omega_2} \Delta U_2 \phi_j dV = \int_{\Omega_2} f_2 \phi_j dV \;\; t \in [t_0, t_f], \\ \int_{\Omega_2} U_2 \phi_j dV = \int_{\Omega_2} U_2^0 \phi_j dV, \;\; t = 0, \;\; j = 1, 2, ..., N-1. \end{aligned} \tag{6}$$

As before, let $\mathbf{u}_I^{(2)}$ correspond to the unknowns on Ω_2 and assume that $f_2 = 0$ in order to simplify the analysis. Then, applying Green's formula to (6) in order to remove the Laplacian operator and letting j run over the interior nodes on Ω_2, we can write the resulting discrete system as:

$$\mathbf{M}_2 \dot{\mathbf{u}}_I^{(2)} + \mathbf{M}_{I\Gamma}^{(2)} \dot{\mathbf{u}}_\Gamma + \mathbf{A}_2 \mathbf{u}_I^{(2)} + \mathbf{A}_{I\Gamma}^{(2)} \mathbf{u}_\Gamma = \mathbf{0}. \tag{7}$$

$\mathbf{A}_2$ and $\mathbf{M}_2$ are the stiffness and the mass matrix for the interior nodes on Ω_2 and they are defined as

$$\begin{aligned} (\mathbf{A}_2)_{ij} = \lambda_2 \int_{\Omega_2} \nabla \phi_i \nabla \phi_j dV, \;\; i, j = 1, 2, ..., N-1, \\ (\mathbf{M}_2)_{ij} = \alpha_2 \int_{\Omega_2} \phi_i \phi_j dV, \;\; i, j = 1, 2, ..., N-1. \end{aligned}$$

The required data from the interface is inserted in the equations by the matrices $\mathbf{A}_{I\Gamma}^{(2)}$ and $\mathbf{M}_{I\Gamma}^{(2)}$. However, the system (4)-(7) is not enough to describe (1). Extending the approach (4)-(7) for the unsteady transmission problem, we will look for an approximation of the normal derivatives on Γ. For this, we consider the interface discretization point $\mathbf{u}_\Gamma$ to be discretized with FDM with respect to the first equation in (1) for $m = 1$ and with FEM with respect to the first equation in (1) for $m = 2$.
On one hand, we use centered finite differences to discretize $\mathbf{u}_\Gamma$ for both first and second order derivatives because this choice forces second order accuracy at the interface point [13, pp. 31]. For this, we need to introduce another unknown $u_2(x_1, t)$ to get

$$\begin{aligned} \lambda_1 \frac{\partial u_1}{\partial n_1} \approx \frac{\lambda_1}{2\Delta x}(u_1(x_N, t) - u_2(x_1, t)), \\ \alpha_1 \dot{\mathbf{u}_\Gamma} + \frac{\lambda_1}{\Delta x^2}(u_1(x_N, t) - 2\mathbf{u}_\Gamma + u_2(x_1, t)) = 0. \end{aligned} \tag{8}$$

Removing $u_2(x_1, t)$ from (8) we get for the following approximation for the normal derivative:

$$\mu_{\text{FDM}} = \mathbf{M}_{\Gamma\Gamma}^{(1)} \dot{\mathbf{u}}_\Gamma + \mathbf{A}_{\Gamma\Gamma}^{(1)} \mathbf{u}_\Gamma + \mathbf{A}_{\Gamma I}^{(1)} \mathbf{u}_I^{(1)}. \tag{9}$$

On the other hand, given the local exact solution u_2, its normal derivative can be written as a linear functional by using Green's formula [20]. Thus,

$$\lambda_2 \int_\Gamma \frac{\partial u_2}{\partial n_2}\phi_j dS = \lambda_2 \int_{\Omega_2} (\Delta u_2 \phi_j + \nabla u_2 \cdot \nabla \phi_j) dV \tag{10}$$
$$= \int_{\Omega_2} (-\alpha_2 \frac{\partial u_2}{\partial t}\phi_j + \lambda_2 \nabla u_2 \cdot \nabla \phi_j) dV.$$

And now, letting j run over the nodes on Γ we obtain the following expressions for the normal derivative:

$$\mu_{\text{FEM}} = \mathbf{M}^{(2)}_{\Gamma\Gamma}\dot{\mathbf{u}}_\Gamma + \mathbf{M}^{(2)}_{\Gamma I}\dot{\mathbf{u}}^{(2)}_I + \mathbf{A}^{(2)}_{\Gamma\Gamma}\mathbf{u}_\Gamma + \mathbf{A}^{(2)}_{\Gamma I}\mathbf{u}^{(2)}_I. \tag{11}$$

Consequently, the equation

$$\mu_{\text{FDM}} + \mu_{\text{FEM}} = 0 \tag{12}$$

completes the system (4)-(7).
Now, we reformulate the coupled equations (4), (7) and (12) into an ODE for the vector of unknowns $\mathbf{u} = (\mathbf{u}^{(1)}_I, \mathbf{u}^{(2)}_I, \mathbf{u}_\Gamma)^T$

$$\tilde{\mathbf{M}}\dot{\mathbf{u}} + \tilde{\mathbf{A}}\mathbf{u} = 0 \tag{13}$$

where

$$\tilde{\mathbf{M}} = \begin{pmatrix} \alpha_1\mathbf{I} & \mathbf{0} & \mathbf{0} \\ \mathbf{0} & \mathbf{M}_2 & \mathbf{M}^{(2)}_{I\Gamma} \\ \mathbf{0} & \mathbf{M}^{(2)}_{\Gamma I} & \mathbf{M}^{(1)}_{\Gamma\Gamma} + \mathbf{M}^{(2)}_{\Gamma\Gamma} \end{pmatrix}, \quad \tilde{\mathbf{A}} = \begin{pmatrix} \mathbf{A}_1 & \mathbf{0} & \mathbf{A}^{(1)}_{I\Gamma} \\ \mathbf{0} & \mathbf{A}_2 & \mathbf{A}^{(2)}_{I\Gamma} \\ \mathbf{A}^{(1)}_{\Gamma I} & \mathbf{A}^{(2)}_{\Gamma I} & \mathbf{A}^{(1)}_{\Gamma\Gamma} + \mathbf{A}^{(2)}_{\Gamma\Gamma} \end{pmatrix}.$$

2.2 Time Discretization

Applying the implicit Euler method with time step Δt to the system (13), we get for the vector of unknowns $\mathbf{u}^{n+1} = (\mathbf{u}^{(1),n+1}_I, \mathbf{u}^{(2),n+1}_I, \mathbf{u}^{n+1}_\Gamma)^T$

$$\mathbf{A}\mathbf{u}^{n+1} = \mathbf{u}^n \tag{14}$$

where $\mathbf{u}^n = (\alpha_1\mathbf{u}^{(1),n}_I,\ \mathbf{M}_2\mathbf{u}^{(2),n}_I + \mathbf{M}^{(2)}_{I\Gamma}\mathbf{u}^n_\Gamma,\ \mathbf{M}^{(2)}_{\Gamma I}\mathbf{u}^{(2),n}_I + \mathbf{M}_{\Gamma\Gamma}\mathbf{u}^n_\Gamma)^T$ and

$$\mathbf{A} = \tilde{\mathbf{M}} - \Delta t\tilde{\mathbf{A}} = \begin{pmatrix} \alpha_1\mathbf{I} - \Delta t\mathbf{A}_1 & \mathbf{0} & -\Delta t\mathbf{A}^{(1)}_{I\Gamma} \\ \mathbf{0} & \mathbf{M}_2 - \Delta t\mathbf{A}_2 & \mathbf{M}^{(2)}_{I\Gamma} - \Delta t\mathbf{A}^{(2)}_{I\Gamma} \\ -\Delta t\mathbf{A}^{(1)}_{\Gamma I} & \mathbf{M}^{(2)}_{\Gamma I} - \Delta t\mathbf{A}^{(2)}_{\Gamma I} & \mathbf{M}_{\Gamma\Gamma} - \Delta t\mathbf{A}_{\Gamma\Gamma} \end{pmatrix},$$

with $\mathbf{M}_{\Gamma\Gamma} = \mathbf{M}^{(1)}_{\Gamma\Gamma} + \mathbf{M}^{(2)}_{\Gamma\Gamma}$ and $\mathbf{A}_{\Gamma\Gamma} = \mathbf{A}^{(1)}_{\Gamma\Gamma} + \mathbf{A}^{(2)}_{\Gamma\Gamma}$.

3 FIXED POINT ITERATION

We now employ a standard Dirichlet-Neumann iteration to solve the discrete system (14). This corresponds to alternatively solving the discretized equations of the transmission problem (1) on Ω_1 with Dirichlet data on Γ and the discretization of (1) on Ω_2 with Neumann data on Γ. Due to the Dirichlet boundary condition, we can compute the solution of (1) on Ω_1 explicitly. However, a system of two equations is needed to find the solution on Ω_2 and Γ simultaneously due to the Neumann boundary condition.
Applying this to (14), one gets for the k-th iteration the two equation systems

$$(\alpha_1 \mathbf{I} - \Delta t \mathbf{A}_1)\mathbf{u}_I^{(1),n+1,k+1} = \Delta t \mathbf{A}_{I\Gamma}^{(1)} \mathbf{u}_\Gamma^{n+1,k} + \alpha_1 \mathbf{u}_I^{(1),n}, \tag{15}$$

$$\hat{\mathbf{A}}\hat{\mathbf{u}}^{k+1} = \hat{\mathbf{u}}^k, \tag{16}$$

to be solved in succession. Here,

$$\hat{\mathbf{A}} = \begin{pmatrix} \mathbf{M}_2 - \Delta t \mathbf{A}_2 & \mathbf{M}_{I\Gamma}^{(2)} - \Delta t \mathbf{A}_{I\Gamma}^{(2)} \\ \mathbf{M}_{\Gamma I}^{(2)} - \Delta t \mathbf{A}_{\Gamma I}^{(2)} & \mathbf{M}_{\Gamma\Gamma}^{(2)} - \Delta t \mathbf{A}_{\Gamma\Gamma}^{(2)} \end{pmatrix}, \quad \hat{\mathbf{u}}^{k+1} = \begin{pmatrix} \mathbf{u}_I^{(2),n+1,k+1} \\ \mathbf{u}_\Gamma^{n+1,k+1} \end{pmatrix}$$

and

$$\hat{\mathbf{u}}^k = \begin{pmatrix} \mathbf{M}_2 \mathbf{u}_I^{(2),n} + \mathbf{M}_{I\Gamma}^{(2)} \mathbf{u}_\Gamma^n \\ \Delta t \mathbf{A}_{\Gamma I}^{(1)} \mathbf{u}_I^{(1),n+1,k+1} - (\mathbf{M}_{\Gamma\Gamma}^{(1)} - \Delta t \mathbf{A}_{\Gamma\Gamma}^{(1)}) \mathbf{u}_\Gamma^{n+1,k} + \mathbf{M}_{\Gamma I}^{(2)} \mathbf{u}_I^{(2),n} + \mathbf{M}_{\Gamma\Gamma} \mathbf{u}_\Gamma^n \end{pmatrix}$$

with some initial condition, here $\mathbf{u}_\Gamma^{n+1,0} = \mathbf{u}_\Gamma^n$. The iteration is terminated according to the standard criterion $\|\mathbf{u}_\Gamma^{k+1} - \mathbf{u}_\Gamma^k\| \leq \tau$ where τ is a user defined tolerance [2].
We now rewrite (15)-(16) as an iteration for $\mathbf{u}_\Gamma^{n+1}$. To this end, we isolate the term $\mathbf{u}_I^{(1),n+1,k+1}$ from (15) and $\mathbf{u}_I^{(2),n+1,k+1}$ from the first equation in (16):

$$\mathbf{u}_I^{(1),n+1,k+1} = (\alpha_1 \mathbf{I} - \Delta t \mathbf{A}_1)^{-1} (\Delta t \mathbf{A}_{I\Gamma}^{(1)} \mathbf{u}_\Gamma^{n+1,k} + \alpha_1 \mathbf{u}_I^{(1),n}), \tag{17}$$

$$\mathbf{u}_I^{(2),n+1,k+1} = (\mathbf{M}_2 - \Delta t \mathbf{A}_2)^{-1} (-(\mathbf{M}_{I\Gamma}^{(2)} - \Delta t \mathbf{A}_{I\Gamma}^{(2)}) \mathbf{u}_\Gamma^{n+1,k+1} + \mathbf{M}_2 \mathbf{u}_I^{(2),n} + \mathbf{M}_{I\Gamma}^{(2)} \mathbf{u}_\Gamma^n). \tag{18}$$

Inserting (17) and (18) into the second equation of (16) one obtains the iteration $\mathbf{u}_\Gamma^{n+1,k+1} = \Sigma \mathbf{u}_\Gamma^{n+1,k} + \psi$, with iteration matrix

$$\Sigma = -{\mathbf{S}^{(2)}}^{-1} \mathbf{S}^{(1)}, \tag{19}$$

where

$$\mathbf{S}^{(1)} = (\mathbf{M}_{\Gamma\Gamma}^{(1)} - \Delta t \mathbf{A}_{\Gamma\Gamma}^{(1)}) - \Delta t^2 \mathbf{A}_{\Gamma I}^{(1)} (\alpha_1 \mathbf{I} - \Delta t \mathbf{A}_1)^{-1} \mathbf{A}_{I\Gamma}^{(1)}, \tag{20}$$

$$\mathbf{S}^{(2)} = (\mathbf{M}_{\Gamma\Gamma}^{(2)} - \Delta t \mathbf{A}_{\Gamma\Gamma}^{(2)}) - (\mathbf{M}_{\Gamma I}^{(2)} - \Delta t \mathbf{A}_{\Gamma I}^{(2)})(\mathbf{M}_2 - \Delta t \mathbf{A}_2)^{-1} (\mathbf{M}_{I\Gamma}^{(2)} - \Delta t \mathbf{A}_{I\Gamma}^{(2)}), \tag{21}$$

and ψ are other terms non dependent on $\mathbf{u}_\Gamma^{n+1,k}$.
Thus, the Dirichlet-Neumann iteration is a linear iteration and the rate of convergence is described by the spectral radius of the iteration matrix.

4 ANALYSIS

In this section, we study the iteration matrix Σ for an specific FDM-FEM discretizations. We will give an exact formula which computes the convergence rates. The behavior of the rates when approaching both the continuous case in time and space are also given.
Specifically, we consider $\Omega_1 = [0,1]$, $\Omega_2 = [1,2]$ and the standard piecewise-linear polynomials

$$\phi_k(x) := \left\{ \begin{array}{cc} \frac{x-x_{k-1}}{x_k-x_{k-1}}, & \text{if } x_{k-1} < x \leq x_k \\ \frac{x_{k+1}-x}{x_{k+1}-x_k}, & \text{if } x_k < x \leq x_{k+1} \\ 0, & \text{otherwise} \end{array} \right\} \tag{22}$$

as test functions on Ω_2.
If we consider $\mathbf{e}_j = \begin{pmatrix} 0 & \cdots & 0 & 1 & 0 & \cdots & 0 \end{pmatrix}^T \in \mathbb{R}^N$ where the only nonzero entry is located at the j-th position, the discretization matrices are given by

$$\mathbf{A}_m = \frac{\lambda_m}{\Delta x^2} \begin{pmatrix} -2 & 1 & & 0 \\ 1 & -2 & \ddots & \\ & \ddots & \ddots & 1 \\ 0 & & 1 & -2 \end{pmatrix}, \quad \mathbf{M}_2 = \frac{\alpha_2}{6} \begin{pmatrix} 4 & 1 & & 0 \\ 1 & 4 & \ddots & \\ & \ddots & \ddots & 1 \\ 0 & & 1 & 4 \end{pmatrix},$$

$$\mathbf{M}^{(1)}_{\Gamma\Gamma} = \frac{\alpha_1}{2}, \ \mathbf{M}^{(2)}_{\Gamma\Gamma} = \frac{2\alpha_2}{6}, \ \mathbf{A}^{(m)}_{\Gamma\Gamma} = -\frac{\lambda_m}{\Delta x^2}, \ m = 1,2.$$
$$\mathbf{A}^{(1)}_{I\Gamma} = \frac{\lambda_1}{\Delta x^2}\mathbf{e}_N, \ \mathbf{A}^{(2)}_{I\Gamma} = \frac{\lambda_2}{\Delta x^2}\mathbf{e}_1, \ \mathbf{M}^{(2)}_{I\Gamma} = \frac{\alpha_2}{6}\mathbf{e}_1,$$
$$\mathbf{A}^{(1)}_{\Gamma I} = \frac{\lambda_1}{\Delta x^2}\mathbf{e}^T_N, \ \mathbf{A}^{(2)}_{\Gamma I} = \frac{\lambda_2}{\Delta x^2}\mathbf{e}^T_1, \ \mathbf{M}^{(2)}_{\Gamma I} = \frac{\alpha_2}{6}\mathbf{e}^T_1.$$

where $\Delta x = 1/(N+1)$ and $\mathbf{A}_m$, $\mathbf{M}_2 \in \mathbb{R}^{N\times N}$, $\mathbf{A}^{(m)}_{I\Gamma}$, $\mathbf{M}^{(2)}_{I\Gamma} \in \mathbb{R}^{N\times 1}$ and $\mathbf{A}^{(m)}_{\Gamma I}$, $\mathbf{M}^{(2)}_{\Gamma I} \in \mathbb{R}^{1\times N}$ for $m = 1,2$.
Note that the iteration matrix Σ is just a real number in this case and thus its spectral radius is its modulus. The goal now is to compute $\mathbf{S}^{(1)}$ and $\mathbf{S}^{(2)}$. Inserting the corresponding matrices specified in (19) we have

$$\begin{aligned} \mathbf{S}^{(1)} &= \left(\frac{\alpha_1}{2} + \Delta t \frac{\lambda_1}{\Delta x^2}\right) - \Delta t^2 \frac{\lambda_1^2}{\Delta x^4} \mathbf{e}_N^T (\alpha_1 \mathbf{I} - \Delta t \mathbf{A}_1)^{-1} \mathbf{e}_N \\ &= \left(\frac{\alpha_1}{2} + \Delta t \frac{\lambda_1}{\Delta x^2}\right) - \Delta t^2 \frac{\lambda_1^2}{\Delta x^4} \alpha^1_{NN}, \end{aligned} \tag{23}$$

$$\begin{aligned} \mathbf{S}^{(2)} &= \left(\frac{\alpha_2}{3} + \Delta t \frac{\lambda_2}{\Delta x^2}\right) - \left(\frac{\alpha_2}{6} - \Delta t \frac{\lambda_2}{\Delta x^2}\right)^2 \mathbf{e}_1^T (\mathbf{M}_2 - \Delta t \mathbf{A}_2)^{-1} \mathbf{e}_1 \\ &= \left(\frac{\alpha_2}{3} + \Delta t \frac{\lambda_2}{\Delta x^2}\right) - \left(\frac{\alpha_2}{6} - \Delta t \frac{\lambda_2}{\Delta x^2}\right)^2 \alpha^2_{11}, \end{aligned} \tag{24}$$

where α_{ij}^1 represent the entries of the matrix $(\alpha_1\mathbf{I}-\Delta t\mathbf{A}_1)^{-1}$ and α_{ij}^2 the entries of the matrix $(\mathbf{M}_m-\Delta t\mathbf{A}_m)^{-1}$ for $i,j=1,...,N$. Observe that the matrices $(\alpha_1\mathbf{I}-\Delta t\mathbf{A}_1)$ and $(\mathbf{M}_2-\Delta t\mathbf{A}_2)$ are tridiagonal Toeplitz matrices but their inverses are full matrices. The computation of the exact inverses is based on a recursive formula which runs over the entries [6] and consequently, it is not trivial how to find α_{NN}^1 and α_{11}^2 this way.
Due to these difficulties, we propose to rewrite the matrices $(\alpha_1\mathbf{I}-\Delta t\mathbf{A}_1)^{-1}$ and $(\mathbf{M}_m-\Delta t\mathbf{A}_m)^{-1}$ in terms of their eigendecomposition:

$$(\alpha_1\mathbf{I}-\Delta t\mathbf{A}_1)^{-1}=\left[\text{tridiag}\left(-\frac{\lambda_1\Delta t}{\Delta x^2},\frac{\alpha_1\Delta x^2+2\lambda_1\Delta t}{\Delta x^2},-\frac{\lambda_1\Delta t}{\Delta x^2}\right)\right]^{-1}=\mathbf{V}\Lambda_1^{-1}\mathbf{V}, \tag{25}$$

$$(\mathbf{M}_2-\Delta t\mathbf{A}_2)^{-1}=\left[\text{tridiag}\left(\frac{\alpha_2\Delta x^2-6\lambda_2\Delta t}{6\Delta x^2},\frac{2\alpha_2\Delta x^2+6\lambda_2\Delta t}{3\Delta x^2},\frac{\alpha_2\Delta x^2-6\lambda_2\Delta t}{6\Delta x^2}\right)\right]^{-1}=\mathbf{V}\Lambda_2^{-1}\mathbf{V}, \tag{26}$$

where the matrix $\mathbf{V}$ has the eigenvectors of any symmetric tridiagonal matrix as a columns and the matrices Λ_1, Λ_2 are a diagonal matrices having the eigenvalues of $\alpha_1\mathbf{I}-\Delta t\mathbf{A}_1$ and $\mathbf{M}_2-\Delta t\mathbf{A}_2$ as entries. These are known and given e.g. in [15, pp. 514-516]

$$\begin{aligned} v_{ij}&=\frac{1}{\sum_{k=1}^N\sin^2\left(\frac{k\pi}{N+1}\right)}\sin\left(\frac{ij\pi}{N+1}\right)\quad\text{for } i,j=1,...,N,\\ \lambda_j^1&=\frac{1}{\Delta x^2}\left(\alpha_1\Delta x^2+2\lambda_1\Delta t-2\lambda_1\Delta t\cos\left(\frac{j\pi}{N+1}\right)\right),\\ \lambda_j^2&=\frac{1}{3\Delta x^2}\left(2\alpha_2\Delta x^2+6\lambda_2\Delta t+(\alpha_2\Delta x^2-6\lambda_2\Delta t)\cos\left(\frac{j\pi}{N+1}\right)\right)\\ &\qquad\qquad\text{for } j=1,...,N\ \ m=1,2. \end{aligned} \tag{27}$$

The entries α_{NN}^1 and α_{11}^2 of the matrices $(\alpha_1\mathbf{I}-\Delta t\mathbf{A}_1)^{-1}$ and $(\mathbf{M}_2-\Delta t\mathbf{A}_2)^{-1}$, respectively, are now computed through their eigendecomposition resulting in

$$\alpha_{NN}^1=\frac{\sum_{i=1}^N\frac{1}{\lambda_i^1}\sin^2\left(\frac{i\pi N}{N+1}\right)}{\sum_{i=1}^N\sin^2\left(\frac{i\pi}{N+1}\right)}=\frac{s_1}{\sum_{i=1}^N\sin^2(i\pi\Delta x)}, \tag{28}$$

$$\alpha_{11}^2=\frac{\sum_{i=1}^N\frac{1}{\lambda_i^2}\sin^2\left(\frac{i\pi}{N+1}\right)}{\sum_{i=1}^N\sin^2\left(\frac{i\pi}{N+1}\right)}=\frac{s_2}{\sum_{i=1}^N\sin^2(i\pi\Delta x)}, \tag{29}$$

with

$$s_1=\sum_{i=1}^N\frac{\Delta x^2\sin^2(i\pi\Delta x)}{\alpha_1\Delta x^2+2\lambda_1\Delta t(1-\cos(i\pi\Delta x))}, \tag{30}$$

$$s_2=\sum_{i=1}^N\frac{3\Delta x^2\sin^2(i\pi\Delta x)}{2\alpha_2\Delta x^2+6\lambda_2\Delta t+(\alpha_2\Delta x^2-6\lambda_2\Delta t)\cos(i\pi\Delta x)}. \tag{31}$$

Now, inserting (28) and (29) into (23) and (24) we get for $\mathbf{S}^{(1)}$ and $\mathbf{S}^{(2)}$,

$$\mathbf{S}^{(1)} = \frac{\alpha_1\Delta x^2 + 2\lambda_1\Delta t}{2\Delta x^2} - \frac{\lambda_1^2\Delta t^2}{\Delta x^4}\frac{s_1}{\sum_{i=1}^{N}\sin^2(i\pi\Delta x)}, \tag{32}$$

$$\mathbf{S}^{(2)} = \frac{\alpha_2\Delta x^2 + 3\lambda_2\Delta t}{3\Delta x^2} - \frac{(\alpha_2\Delta x^2 - 6\lambda_2\Delta t)^2}{36\Delta x^4}\frac{s_2}{\sum_{i=1}^{N}\sin^2(i\pi\Delta x)}. \tag{33}$$

With this we obtain an explicit formula for the spectral radius of the iteration matrix Σ as a function of Δx and Δt:

$$\begin{aligned}\rho(\Sigma) = |\Sigma| = |{\mathbf{S}^{(2)}}^{-1}\mathbf{S}^{(1)}|\\ = \left(\frac{\alpha_2\Delta x^2 + 3\lambda_2\Delta t}{3\Delta x^2} - \frac{(\alpha_2\Delta x^2 - 6\lambda_2\Delta t)^2}{36\Delta x^4}\frac{s_1}{\sum_{i=1}^{N}\sin^2(i\pi\Delta x)}\right)^{-1}\\ \cdot\left(\frac{\alpha_1\Delta x^2 + 2\lambda_1\Delta t}{2\Delta x^2} - \frac{\lambda_1^2\Delta t^2}{\Delta x^4}\frac{s_2}{\sum_{i=1}^{N}\sin^2(i\pi\Delta x)}\right).\end{aligned} \tag{34}$$

To simplify this, the finite sum $\sum_{i=1}^{N}\sin^2(i\pi\Delta x)$ can be computed. We first rewrite the sum of squared sinus into a sum of cosinus using the identity $\sin^2(x/2) = (1-\cos(x))/2$. Then, the resulting sum can be converted into a geometric sum using Euler's formula:

$$\begin{aligned}\sum_{j=1}^{N}\sin^2(j\pi\Delta x) &= \frac{1-\Delta x}{2\Delta x} - \frac{1}{2}\sum_{j=1}^{N}\cos(2j\pi\Delta x)\\ &= \frac{1-\Delta x}{2\Delta x} - \frac{1}{2}Re\left(\sum_{j=1}^{N}e^{2ij\pi\Delta x}\right)\\ &= \frac{1-\Delta x}{2\Delta x} - \frac{1}{2}Re\left(\frac{e^{2i\pi\Delta x}\left(1-e^{2iN\pi\Delta x}\right)}{1-e^{2i\pi\Delta x}}\right)\\ &= \frac{2\Delta x\cos^2(\pi\Delta x) - 2\Delta x + 1}{2\Delta x}\end{aligned} \tag{35}$$

Inserting (35) into (34) we get after some manipulations

$$|\Sigma| = \frac{9\Delta x(\alpha_1\Delta x^2 + 2\lambda_1\Delta t)(2\Delta x\cos^2(\pi\Delta x) - 2\Delta x + 1) - 36\lambda_1^2\Delta t^2 s_1}{3\Delta x(2\alpha_2\Delta x^2 + 6\lambda_2\Delta t)(2\Delta x\cos^2(\pi\Delta x) - 2\Delta x + 1) - (\alpha_2\Delta x^2 - 6\lambda_2\Delta t)^2 s_2}. \tag{36}$$

This is a computable formula that gives exactly the convergence rates of the Dirichlet-Neumann iteration for given Δx, Δt, α_m and λ_m, $m = 1, 2$.
We are now interested in the asymptotics of (36). In particular, we want to know the behaviour of (36) when Δt or Δx tend to 0. However, the denominators of (30) and (31) become zero when Δx tends to 0. To solve this problem, we reformulate (36) in terms of $c = \Delta t/\Delta x^2$. To get that, we multiply (36) by $1/\Delta x^2$ both in the numerator and denominator getting

$$|\Sigma| = \frac{9\Delta x(\alpha_1 + 2\lambda_1 c)(2\Delta x \cos^2(\pi\Delta x) - 2\Delta x + 1) - 36\Delta x \lambda_1^2 c^2 s_1'}{3(2\alpha_2 + 6\lambda_2 c)(2\Delta x \cos^2(\pi\Delta x) - 2\Delta x + 1) - \Delta x(\alpha_2 - 6\lambda_2 c)^2 s_2'} \tag{37}$$

where

$$s_1' = \sum_{i=1}^{N} \frac{\sin^2(i\pi\Delta x)}{\alpha_1 + 2\lambda_1 c(1 - \cos(i\pi\Delta x))}, \tag{38}$$

$$s_2' = \sum_{i=1}^{N} \frac{3\sin^2(i\pi\Delta x)}{2\alpha_2 + 6\lambda_2 c + (\alpha_2 - 6\lambda_2 c)\cos(i\pi\Delta x)}. \tag{39}$$

for $m = 1, 2$.
Computing the limits of (37) when $c \to 0$ and $c \to \infty$ we get

$$\begin{aligned} \lim_{c\to 0} |\Sigma| &= \frac{9\alpha_1(2\Delta x \cos^2(\pi\Delta x) - 2\Delta x + 1)}{6\alpha_2(2\Delta x \cos^2(\pi\Delta x) - 2\Delta x + 1) - \Delta x \alpha_2^2 \sum_{i=1}^{N} \frac{3\sin^2(i\pi\Delta x)}{\alpha_2(2+\cos(i\pi\Delta x))}} \\ &= \frac{3\alpha_1(2\Delta x \cos^2(\pi\Delta x) - 2\Delta x + 1)}{\alpha_2\left(2(2\Delta x \cos^2(\pi\Delta x) - 2\Delta x + 1) - \Delta x \sum_{i=1}^{N} \frac{\sin^2(i\pi\Delta x)}{2+\cos(i\pi\Delta x)}\right)} =: \gamma, \end{aligned} \tag{40}$$

$$\begin{aligned} \lim_{c\to\infty} |\Sigma| &= \lim_{c\to\infty} \frac{18\lambda_1 c(2\Delta x \cos^2(\pi\Delta x) - 2\Delta x + 1) - 36(\lambda_1 c)^2 \sum_{i=1}^{N} \frac{\sin^2(i\pi\Delta x)}{2\lambda_1 c(1-\cos(i\pi\Delta x))}}{18\lambda_2 c(2\Delta x \cos^2(\pi\Delta x) - 2\Delta x + 1) - 36(\lambda_2 c)^2 \sum_{i=1}^{N} \frac{3\sin^2(i\pi\Delta x)}{6\lambda_2 c(1-\cos(i\pi\Delta x))}} \\ &= \frac{\lambda_1\left((2\Delta x \cos^2(\pi\Delta x) - 2\Delta x + 1) + \Delta x - 1 - \Delta x \sum_{i=1}^{N} \cos(i\pi\Delta x)\right)}{\lambda_2\left((2\Delta x \cos^2(\pi\Delta x) - 2\Delta x + 1) + \Delta x - 1 - \Delta x \sum_{i=1}^{N} \cos(i\pi\Delta x)\right)} = \frac{\lambda_1}{\lambda_2} =: \delta. \end{aligned} \tag{41}$$

The result obtained in (41) matches with [16] and strong jumps in the thermal conductivities of the materials placed in Ω_1 and Ω_2 will imply fast convergence. This is the case when modelling thermal fluid structure interaction, where usually a compressible fluid with low thermal conductivity and density is coupled with a structure having higher thermal conductivity and density. However, the result in (40) does not only depend on the ratio of α_m, $m = 1, 2$. It also depends on Δx, and therefore, in the case of mixed discretizations more factors affect the rates. We will compare (40) with the results obtained in [16] in more details in the next section.

5 NUMERICAL RESULTS

In this section we present a set of numerical experiments designed to show how (36) computes the convergence rates. We also show that the theoretical asymptotics deduced both in (40) and (41) match with the numerical experiments.
Figure 1 shows the cases 1 and 2 specified in table 1. The circles correspond to $\rho(\Sigma)$, the crosses to the experimental convergence rates and the dashed line to the corresponding asymptotic (γ when $\Delta t \to 0$ and δ when $\Delta x \to 0$). Notice that the method does not converge for some cases. Nevertheless $|\Sigma|$ describes the convergence rate and γ and δ their asymptotics.

Case	D_1	D_2	λ_1	λ_2	δ	γ	γ_{FEM}	$1.74 \cdot \gamma_{\text{FEM}}$
1	1	0.3	0.3	1	0.3	0.26	0.15	0.16
2	0.3	1	0.3	1	0.3	1.04	0.6	1.04
3	1	0.5	0.3	1	0.3	0.16	0.09	0.16
4	0.5	1	0.3	1	0.3	1.73	1	1.74

Table 1: The first four columns contain the input parameters for the different one dimensional test cases. γ and δ are the resulting limits when approaching the continuous case in time and space of the discrete estimator. γ_{FEM} is the semidiscrete limit in time specified in [16] and the last column corresponds to the relation between γ_{FEM} and γ.

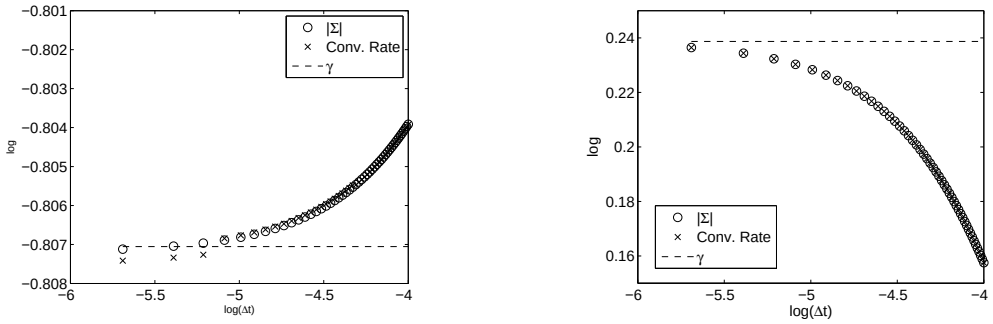

(a) Case 1. (b) Case 2.

Figure 1: Cases 1 and 2 from table 1. The circles correspond to $|\Sigma|$, the crosses to the experimental convergence rates and the dashed line to γ. The curves are restricted to the discrete values $\Delta t = 1e-4/50, 2 \cdot 1e-4/50, ..., 50 \cdot 1e-4/50$ and $\Delta x = 1/20$. One observes how γ describes the behaviour of the convergence rates when we enforce the condition $\Delta t/\Delta x^2 << 1$.

Even though a 2D analysis has not been done, one can expect that a similar analysis will hold due to the results shown in figure 2. To illustrate this, figure 2 shows the experimental convergence rates for cases 1 and 2 in 2D. One observes that the rates in the 2D case have a similar behavior than in the 1D case (figure 1).

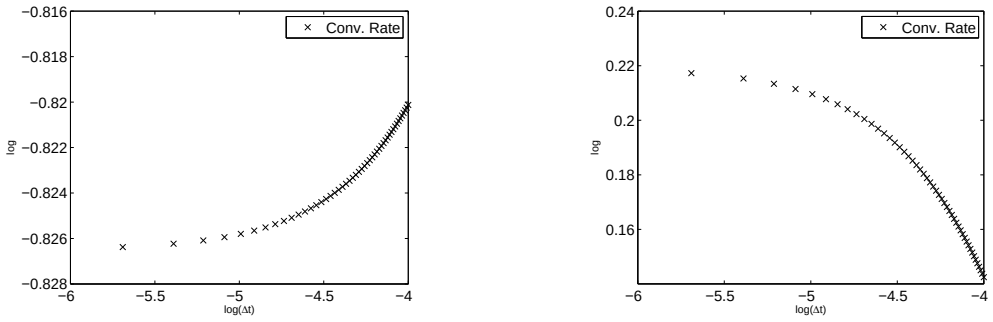

(a) Case 1. (b) Case 2.

Figure 2: The experimental convergence rates in 2D for cases 1 and 2 in table 1. The curves are restricted to the discrete values $\Delta t = 1e-4/50, 2 \cdot 1e-4/50, ..., 50 \cdot 1e-4/50$ and $\Delta x = 1/20$. A similar behaviour to the 1D case is observed here.

Now we want to test if the convergence rates when approaching the continuous case in space have dependency on the thermal diffusivities D_1 and D_2 as predicted in [9] or they do not as

in our analysis. For that, figure 3 shows the cases 1 and 2 from table 1. Here, the thermal conductivities λ_1 and λ_2 are the same in both plots but the thermal diffusivities are switched (meaning that D_1 in case 1 corresponds to D_2 in case 2 and D_2 in case 1 corresponds to D_1 in case 2). We can observe that the asymptotics of the convergence rates do not vary in both plots. This result is consistent with [17] where a similar behaviour was observed for the 2D version of the coupled unsteady transmission problem discretized with finite differences and also with [16] where a 1D and 2D convergence analysis for the unsteady transmission problem discretized with finite elements was performed. Finally, observe that the convergence rate does not vary a lot when we decrease Δx. For a fairly large choice of Δx (for instance $\Delta x = 1/10$), the convergence rates are already quite close to δ.

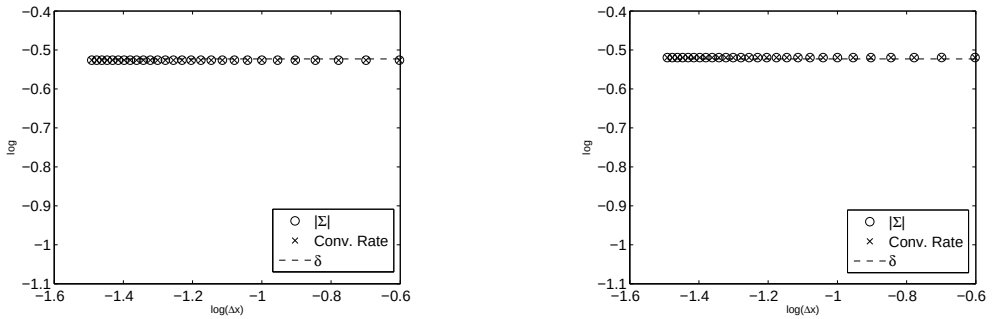

(a) Case 1. (b) Case 2.

Figure 3: Cases 1 and 2 from table 1. The curves are restricted to the discrete values $\Delta x = 1/3, 1/4, ..., 1/30$ and $\Delta t = 100$. One observes how δ describes the behaviour of the convergence rates when we enforce the condition $\Delta t/\Delta x^2 >> 1$.

Before ending this section, we want to present a comparison between the semidiscrete limit in time presented in this paper (γ) and the one computed in [16] when both subdomains Ω_1 and Ω_2 are discretized with finite elements (γ_{FEM}) which was defined as

$$\gamma_{\text{FEM}} := \frac{\alpha_1}{\alpha_2}. \tag{42}$$

Figure 4 and 5 show the comparison between γ and γ_{FEM} for the cases 3 and 4 specified in table 1. One can observe that $\gamma > \gamma_{\text{FEM}}$, and therefore, the method will be slower using mixed discretizations (FDM - FEM) than using pure FEM discretization when approaching the continuous case in time. More in general, from the numerical experiments is possible to observe that

$$\gamma \approx \frac{c_1\alpha_1}{c_2\alpha_2} = \frac{c_1}{c_2}\gamma_{\text{FEM}} \tag{43}$$

with constants $c_1 = 9$ and $c_2 = 5.18$. This phenomena can also been checked in table 1 where this approximation has been included in the last column.

6 CONCLUSIONS AND FURTHER WORK

We have described the Dirichlet-Neumann iteration for the coupling of two heat equations on two identical domains. In particular, the coupled PDE were discretized into a system of algebraic equations using finite differences on Ω_1 and finite elements on Ω_2. Afterwards, a fixed

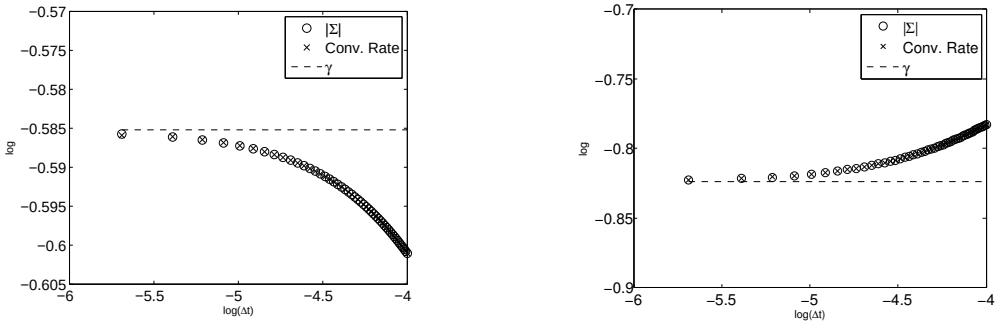

(a) Mixed discretizations (b) FEM discretization

Figure 4: Case 3 from table 1. Comparison between γ (left) and γ_{FEM} (right). The curves are restricted to the discrete values $\Delta t = 1e-4/50, 2\cdot 1e-4/50, ..., 50\cdot 1e-4/50$ and $\Delta x = 1/20$. Observe that $\gamma > \gamma_{\text{FEM}}$ and in particular, $\gamma \approx 1.74\gamma_{\text{FEM}}$.

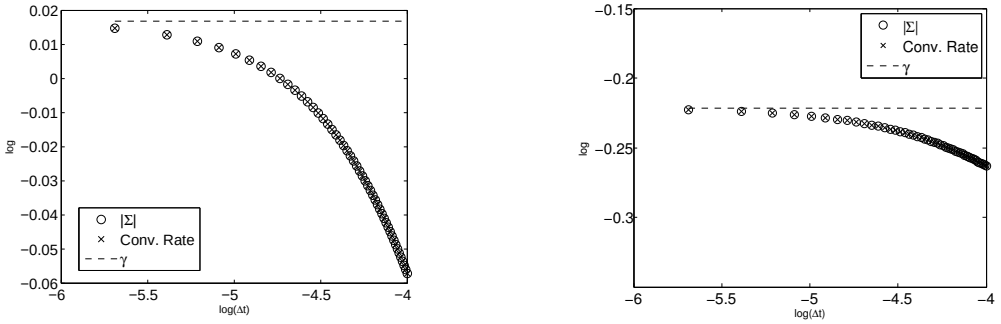

(a) Mixed discretizations (b) FEM discretization

Figure 5: Case 4 from table 1. Comparison between γ (left) and γ_{FEM} (right). The curves are restricted to the discrete values $\Delta t = 1e-4/50, 2\cdot 1e-4/50, ..., 50\cdot 1e-4/50$ and $\Delta x = 1/20$. Observe that $\gamma > \gamma_{\text{FEM}}$ and in particular, $\gamma \approx 1.74\gamma_{\text{FEM}}$.

point iteration was performed and the iteration matrix was found. An exact formula describing the convergence rates is derived. Finally, the limits of the convergence rates when approaching the continuous case either in space ($\delta := \lambda_1/\lambda_2$) or time ($\gamma$) are computed. In the numerical results, we have presented four different test cases which show how the computed asymptotics predict the behaviour of the convergence rates and a comparison with the results of the pure finite element discretization of the problem in [16].

From the first four test cases we conclude that Δx does not strongly affect the convergence rates. However, they are affected by Δt. Moreover, our results show that when approaching the continuous case in space ($\Delta x \to 0$) the convergence rates do not depend on the thermal diffusivities D_1 and D_2 as predicted in [9] for the semidiscrete case. We found the analysis in [9] to be correct and are not sure where the discrepancy comes from, this is subject of further investigation.

From the comparison between γ and γ_{FEM} we can observe that $\gamma > \gamma_{\text{FEM}}$ and more specifically, $\gamma \approx 9\alpha_1/5.18\alpha_2 = 1.74\cdot\gamma_{\text{FEM}}$. This explains why the convergence of the method when approaching the continuous case in time is slower when using the mixed discretizations FDM - FEM with respect to the pure FEM discretization.

There are a variety of future directions for this work. A 2D analysis of this mixed discretization can be done. Another goal would be to analyze the convergence rates of the method using finite

volumes on one domain and finite elements on the other. This is very interesting in the context of fluid structure interaction where the fluid is usually discretized using finite volumes and the structure with finite elements. Another future direction will be to study the convergence speed of an actual non linear application.

REFERENCES

[1] Badia, S., Quaini, A. and Quarteroni, A., *Modular vs. non-modular preconditioners for fluid-structure systems with large added-mass effect*, Comput. Methods Appl. Mech. Engrg., 197 (2008), pp. 4216-4232.

[2] Birken, P., *Termination criteria for inexact fixed point methods*, Numer. Linear Algebra Appl., 22(4) (2015), pp. 702-716.

[3] Birken, P., Gleim, T., Kuhl, D. and Meister, A., *Fast Solvers for Unsteady Thermal Fluid Structure Interaction*, Int. J. Numer. Meth. Fluids, 79(1) (2015), pp. 16-29.

[4] Buchlin, J.M., *Convective Heat Transfer and Infrared Thermography*, J. Appl. Fluid Mech., 3 (2010), pp. 55-62.

[5] Causin, P., Gerbeau, J.F. and Nobile, F., *Added-mass effect in the design of partitioned algorithms for fluid-structure problems*, Comput. Methods Appl. Mech. Engrg., 194 (2005), pp. 4506-4527.

[6] Fonseca, C.M. and Petronilho, J., *Explicit inverses of some tridiagonal matrices*, Linear Algebra and its Applications, 325(1-3) (2001), pp. 7-21.

[7] Giles, M.B., *Stability Analysis of Numerical Interface Conditions in Fluid-Structure Thermal Analysis*, Int. J. Num. Meth. in Fluids, 25 (1997), pp. 421-436.

[8] Heck, U., Fritsching, U. and Bauckhage K., *Fluid flow and heat transfer in gas jet quenching of a cylinder*, International Journal of Numerical Methods for Heat and Fluid Flow, 11 (2001), pp. 36-49.

[9] Henshaw, W.D. and Chand, K.K., *A composite grid solver for conjugate heat transfer in fluid-structure systems*, Journal for Computational Physics, 228 (2009), pp. 2708-3741.

[10] Hinderks, M. and Radespiel, R., *Investigation of Hypersonic Gap Flow of a Reentry Nosecap with Consideration of Fluid Structure Interaction*, AIAA Paper, 6 (2006).

[11] Kowollik, D.S.C., Horst, P. and Haupt, M.C., *Fluid-structure interaction analysis applied to thermal barrier coated cooled rocket thrust chambers with subsequent local investigation of delamination phenomena*, Progress in Propulsion Physics, 4 (2013), pp. 617-636.

[12] Kowollik, D., Tini, V., Reese, S. and Haupt, M., *3D fluid-structure interaction analysis of a typical liquid rocket engine cycle based on a novel viscoplastic damage model*, Int. J. Numer. Meth. Engng, 94 (2013), pp. 1165-1190.

[13] LeVeque, R.J., *Finite Difference Methods for Ordinary and Partial Differential Equations*, Siam, 2007.

[14] Mehta, R.C., *Numerical Computation of Heat Transfer on Reentry Capsules at Mach 5*, AIAA-Paper, 178 (2005).

[15] Meyer, C.D., *Matrix Analysis and Applied Linear Algebra*, 2000.

[16] Monge, A. and Birken, P., *The Dirichlet-Neumann Iteration for Unsteady Thermal Fluid Structure Interaction: Convergence Analysis for Finite Element Discretizations*, SMAI Journal of Computational Mathematics, submitted.

[17] Monge, A. and Birken, P., *Convergence speed of coupling iterations for the unsteady transmission problem*, in B. Schrefler, E. Oate and M. Papadrakakis (Eds), VI International Conference on Computational Methods for Coupled Problems in Science and Engineering, COUPLED PROBLEMS 2015, pp. 452-463.

[18] Quarteroni, A. and Valli, A., *Domain Decomposition Methods for Partial Differential Equations*, Oxford Science Publications, 1999.

[19] Stratton, P., Shedletsky, I. and Lee, M., *Gas Quenching with Helium*, Solid State Phenomena, 118 (2006), pp. 221-226.

[20] Toselli, A. and Widlund, O., *Domain Decomposition Methods - Algorithms and Theory*, Springer, 2004.